# Earth-directed coronal mass ejection shock sheaths as drivers of minor forbush decreases

**Olakunle Ogunjobi[1]*, Ogbos Okike[2], Jude Koffa[3]**

[1]Department of Physics and Astronomy, University of Calgary, Canada
[2]Department of Physics and Astronomy, University of Nigeria Nsukka, Nigeria
[3]Department of Physics, Federal University Lokoja, Nigeria

**Key Points:**

- Small-amplitude Forbush Decreases (FDs), often overlooked, are definitively linked to Earth-directed Coronal Mass Ejections (CMEs).
- Observations of weak scattering in CME sheath regions provide insights into their inclined ellipse cross-sections and orientations.
- CME-driven geomagnetic disturbances can be better predicted with minor FDs, despite their subtlety.

*Department of Physics and Astronomy, University of Calgary

Corresponding author: Ogunjobi, olakunle.ogunjobi@ucalgary.ca

## Abstract

Coronal mass ejections (CMEs) directed toward Earth can modulate cosmic ray fluxes detected on the ground. We provide definitive evidence that even moderately fast CMEs produce small-scale Forbush decreases (FDs) - brief $\leq 3\%$ cosmic ray exclusions over a day. Tracking fronted halo CMEs with coordinated solar imaging and in situ monitoring reveals timing and efficiency signatures statistically linking intensity drops with transient shock passages at ejecta fronts. The reductions originate in weak sheath scattering zones featuring elliptical cross-sections preferentially oriented edge-on to Earth. Connecting properties of these subtle effects to remote CME structure and kinematics elucidates inner heliospheric shock physics below major FDs detection thresholds (CR $\geq 3\%$). This reveals an entirely overlooked category of minor interplanetary perturbations by common solar eruptions insufficient to spark major storms.


## 1 Introduction

Coronal mass ejections (CMEs) represent powerful eruptions of magnetized plasma from the Sun, with masses of $10^13$ up to $10^16$ g (Webb & Howard, 2012). CMEs propagate approximately radially from the Sun (aside from a small eastward deflection caused by solar rotation, (Tsurutani & et al., 2006)), so disk halos are likely to hit Earth. Generally, halo CMEs are said to be frontsided if the location of eruption (also known as the solar source) can be identified on the visible disk, such as the location of H-alpha flares or filament eruptions. A detailed description of how to identify solar sources can be found in (Gopalswamy et al., 2009). With speeds ranging from hundreds to over 2500 km/s, Earth-directed CMEs (also known as interplanetary coronal mass ejections (ICME)) can cause shocks and turbulence in the heliosphere (Gopalswamy et al., 2005). Fast CME events are major drivers of severe space weather at Earth (Dorman et al., 2001), although fundamental questions remain regarding their propagation and geoeffective properties (Green et al., 2018).

When intercepting the Earth, CMEs produce Forbush decreases (FDs) - observed depressions in the cosmic ray intensity. While major FDs involve (CR (%) $\geq 3$) reductions over several days, low-amplitude FDs manifest as intensity drops of only a few percent (CR (%) $\leq 3$), with recovery over $\approx$1 day (Belov et al., 2005; Okike, Alhassan, et al., 2021). The causes of such small-scale events remain unclear, although they require a significant interplanetary perturbation (Lockwood, 1971). Proposed triggers include corotating inter-

action regions (Richardson & Cane, 2010) or small ejecta (Natalya et al., 2020). However, the transient compression signatures indicate possible links to CME sheaths or shock fronts (Li et al., 2015).

Establishing the relationships between small FDs and solar eruptions has key space weather relevance (Menteso et al., 2023). Vršnak et al. (2022) suggested that the responsible structures must feature amplified magnetic fields over background winds based on the cosmic ray deflections. The rareness of minor isolated FDs provides an opportunity to place constraints on the passages of Earth-impacting ejecta (Okike, Alhassan, et al., 2021). Also, advancing knowledge on the relationships between small-amplitude FDs and specific solar eruptions can elucidate multiple aspects of CME propagation physics relevant for forecasting space weather disturbances. The minor cosmic ray reductions require a transient magnetized structure amplified above background solar wind conditions in order to modulate and exclude galactic cosmic rays (Burlaga et al., 1991). Therefore, identifying particular interplanetary drivers of small amplitude FDs constrains the types of solar ejecta capable of achieving weak, temporary geomagnetic perturbations (Natalya et al., 2020). Furthermore, since minor isolated FDs only occasionally arise among background variations, they allow detailed modeling of rare CME shock fronts insufficient to produce major cosmic ray scattering (Okike, Alhassan, et al., 2021). Clarifying whether CME sheaths can yield such effects has key significance for probing acceleration efficiency and shock geometry of common, weaker geo-effective events (Gopalswamy, 2017). This can expand understanding of which aspects of CME development govern ultimate space weather perturbations. Therefore, understanding whether CMEs generate low-amplitude FDs can reveal unique information on shock properties in the inner heliosphere and improve predictions of geomagnetic storm risks.

In this study, we provide the first clear observations directly connecting Earth passage of Coronal Mass Ejections to small-amplitude Forbush decreases through coordinated remote solar imaging and in situ cosmic ray monitoring. Using multi-point measurement analysis to identify correlations between specific CME structures and minor cosmic ray depressions, we investigated whether even moderate solar eruptions were capable of reducing cosmic ray fluxes near Earth by a small but measurable amount.

## 2 Data and techniques

To identify Earth-directed CMEs, we utilized white light coronagraph observations from the Large Angle Spectroscopic Coronagraph (LASCO) instrument aboard the Solar and Heliospheric Observatory (SOHO) spacecraft (Brueckner et al., 1995). LASCO provides continuous monitoring of CME events propagating in the plane of the sky from 2.5 to 32 solar radii. We established an initial set of 51 front-side full halo CMEs during 1996-2023. A list of these events is available through the Goddard Space Flight Center (GSFC)/National Aeronautics and Space Administration (NASA) interface as part of the SOHO/LASCO catalog: `https://cdaw.gsfc.nasa.gov/CME_list/`.

We tracked the propagation of these CMEs to Earth using plasma parameters provided by OMNI database (`https://omniweb.gsfc.nasa.gov/cgi/nx1.cgi`). The data set was created by interspersing, after cross-normalization, field and plasma data from several spacecraft that contributed measurements (King & Papitashvili, 2005). This database provides measurements of near-Earth solar wind, magnetic field, and plasma parameters obtained from different instruments. Geophysical parameters included in the database serve as a proxy for solar wind conditions at Earth's bow shock nose ( 1AU). We derived the timeseries proxy for CME-related disturbances based on measurements of solar wind density from the OMNI database. So, for a minor FD to be accepted, there must be a corresponding density jump at the time of event onset. Density jumps occur when the solar wind rapidly transitions from a region of lower proton density to a region of higher proton density. In this case, we calculated the density jump by subtracting the initial average density from the event average density.

As a means of connecting Earth-arriving ICME events with Forbush decreases (FDs), cosmic ray intensity (`https://www.nmdb.eu/nest/`) was analyzed from the Calgary (CALG) and Oulu neutron monitors (NMs) within the period surrounding the established CME impact times. Since directional anisotropies always cause serious interpretation problems from a single NM, we have used two monitors from different locations. It is important to note that Oulu is located at the directional conjugate of SANAE IV and Halley in the Antarctica. Focusing on isolated, stand-alone FDs, we identified minor intensity depressions under 3% amplitude occurring within $\pm 1$ day of the ICME arrival. Figure 1 shows a schematic major and minor FD event as defined in this study. This definition enabled us to identify 23

halo CME events (see Table 1) during 1996-2023 in which the OMNI data clearly indicated ejecta passage at Earth, while the NM data clearly indicated a significant reduction in CR (%) intensity of ≤3. Here, the FD Amplitude represents the magnitude of the cosmic ray intensity drop relative to the background levels of the specific NM station. Thus, FD events with both positive and negative amplitudes indicate whether suppression or enhancement were observed during each interplanetary transient passage. The practice of treating FD amplitudes as positive-definite percentages has been cemented by Lockwood (1971) and Natalya et al. (2020).

**Table 1.** Date, speed, and arrival time parameters for subset of 23 halo CME events

| Event | FD Time [a] | ICME Speed (km/s) | Density jump | $FD_{SEA}$ (%)[b] |
|---|---|---|---|---|
| 1 | 1998-04-23 | 1255 | 39.20 | -0.45 |
| 2 | 1998-12-14 | 1300 | 2.40 | 0.22 |
| 3 | 1998-06-03 | 1150 | 19.30 | 0.19 |
| 4 | 1999-02-23 | 1319 | 3.20 | -0.18 |
| 5 | 1999-12-19 | 1208 | 1.90 | -1.03 |
| 6 | 2000-02-02 | 1091 | 3.20 | 0.2 |
| 7 | 2001-03-13 | 1185 | 4.20 | 0.19 |
| 8 | 2002-02-15 | 1309 | 4.40 | 0.17 |
| 9 | 2004-05-15 | 1283 | 6.40 | -0.12 |
| 10 | 2004-12-15 | 1135 | 8.20 | 0.18 |
| 11 | 2005-03-07 | 1311 | 10.40 | -0.1 |
| 12 | 2005-06-13 | 1241 | 6.50 | 0.19 |
| 13 | 2005-12-31 | 1292 | 3.10 | -1.65 |
| 14 | 2006-01-01 | 1283 | 15.20 | 0.19 |
| 15 | 2022-10-01 | 1134 | 2.50 | 0.18 |
| 16 | 2023-01-02 | 1285 | 1.80 | -0.13 |
| 17 | 2023-01-31 | 1189 | 2.20 | 0.18 |
| 18 | 2023-02-10 | 1404 | 2.50 | -0.14 |
| 19 | 2023-02-23 | 1322 | 6.00 | -0.11 |
| 20 | 2023-03-08 | 1254 | 7.30 | -0.16 |
| 21 | 2023-04-20 | 1151 | 5.20 | 0.19 |
| 22 | 2023-05-15 | 1255 | 1.90 | 0.21 |
| 23 | 2023-07-14 | 1265 | 25.40 | -0.23 |

[a] at ±1 day ICME arrival Earth.
[b] Based on medidan average of CALG NM.

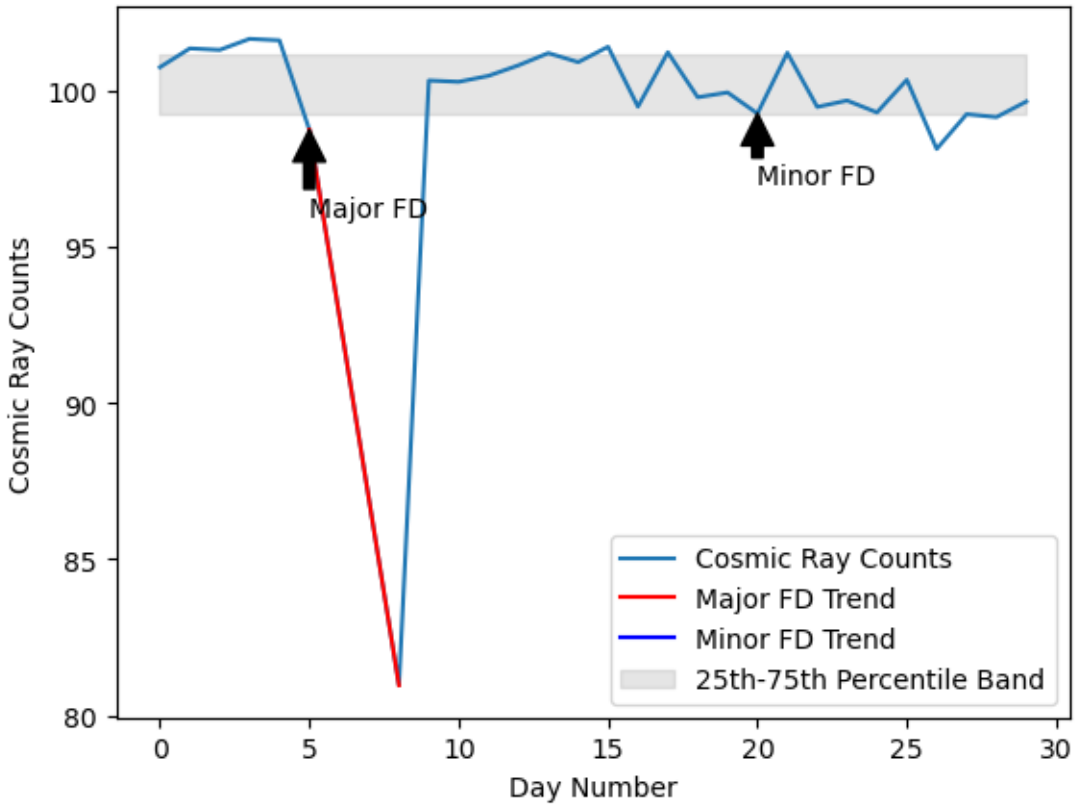


**Figure 1.** The schematic profile of major and minor FD event as defined in this study.

Superposed Epoch Analysis (SEA) was used to determine the statistical significance and trend of 23 minor FDs. In noisy data, SEA helps reveal consistent responses, relative to some repeatable phenomenon (Chree, 1908; Morley et al., 2010; Boakes et al., 2011; Walton & Murphy, 2022; Ogunjobi et al., 2014). All variables at a given time relative to the epoch form a sample of events at that lag (?, ?). This is based on timeseries extracted from a window around the minor FD epoch. Averaging the data at each time lag cancels out fluctuations not consistent with the epoch. Although this is a powerful technique, care should be taken in interpreting it, since a consistent response about an epoch does not suggest causality. Epoch selection bias can also lead to difficult-to-interpret results (Ogunjobi et al., 2014). Our study uses the median as a measure of central tendency, since it is robust and unaffected by outliers. In addition, we present an interquartile range (IQR) as a reliable measure of data spread. Based on a relatively small sample of only 23 events, we calculated bootstrapped 95% confidence intervals (CIs) for the median and IQR (?, ?; Morley et al., 2010). This approach provided the first coordinated remote-sensing and in-situ observations linking Earth-directed CMEs to small transient decreases in the cosmic ray intensity. With clear FD signatures timed with ejecta passages, we quantitatively assess the role of CME-driven shocks in generating minor cosmic ray modulation.

## 3 Results and analysis

### 3.1 Case study

Case studies from CALG NM and Oulu NM are presented. Analysis of minor FD events occurring during different solar cycles on 23 March 1998 and 31 December 2005 is presented. In order to better understand how solar transients affect the intensity of heliospheric cosmic rays, the individual case studies serve as illustrated examples of how specific shock drivers influence cosmic ray modulations.

#### *3.1.1 CALG NM*

We present in Figure 2 an individual case study of minor FD event of 23 March 1998 from CALG NM with specific shock arrival dynamics. The precise timing can be traced to propagating fields associated with solar activity, rather than stochastic changes in interstellar currents. Figure 2 (first panel) shows the solar wind density jump at the onset of

the minor FD. These density enhancements can be attributed to interplanetary shock waves generated by the fronted CMEs. During the propagation of the shock front through the solar wind, a compression region is created, resulting in an increase in density. In addition, the reversal of the SYM/H indices (Figure 2 (second panel)) at the peak of the solar wind density indicates that these parameters have a multifaceted relationship. A distinct reversal of the SYM/H indices occurs concurrently with the maximum density of the solar wind. A complex interplay between solar wind dynamics, geomagnetic disturbances, and cosmic ray modulation is suggested by this synchronization. In Figure 2 (third panel), the density jump coincides with the onset of the minor FD, which precedes the main phase of the minor FDs. A solar wind density jump serves as a crucial precursor, indicating the initiation of a subsequent minor FD event. The CALG NM station recorded a singular, isolated cosmic ray depression on 23 March 1998 which can be interpreted as a rare example of minor space weather events. A concurrent interplanetary density profile overlaying the CME arrival window (Tokumaru et al. 2017) reveals a modulated drop in galactic ray accessibility within hours of the estimated shock front encounter. It is evident from the cosmic ray count profiles that the heliospheric environment is affected by propagating shock structures during the period of FD events. For clarity, the vertical dash line in this figure (Figure 2) indicates the shock arrival, highlighting its relation to the observed modulation of FD.

As shown in Figure 3, this trend continues, but with different magnitudes. Variations in parameters observed between the events on 23 March 1998 and 31 December 2005 can be attributed to several factors, including the solar cycle effect and inherent variability in solar and interplanetary conditions. The years 1998 and 2005 fall within different phases of the solar cycle. There is a waxing and waning in the activity of the solar cycle, affecting both the frequency and intensity of space weather events such as the CMEs. The event in 1998 occurred during the ascending phase of Solar Cycle 23, near the solar maximum. Increased solar activity results in more energetic CMEs and stronger interplanetary shocks, resulting in a higher density jump at solar maximum. The observed density jump of 38 $\mathrm{ncm}^{-3}$ suggests significant solar activity during this period, with a negative SYM/H index (-60 nT) indicating magnetospheric ring current decay. The minor FD amplitude of -0.5 may be caused by the increased solar activity affecting cosmic ray modulation. The 2005 event, on the other hand, occurred during the declining phase of Solar Cycle 23 as the sun approached its minimum. A solar minimum is characterized by reduced solar activity and fewer and less

179 energetic CMEs, resulting in a lower density jump. The observed density jump of 3.1 $ncm^{-3}$
180 and small depression in SYM/H indices suggest that a milder solar disturbance has been
181 observed over the course of this period. During solar minimum, the more negative minor
182 FD amplitude of -1 may be comparatively stronger due to the lower background cosmic ray
183 modulation. Other aspects of solar dynamics, such as the orientation and strength of the
184 interplanetary magnetic field, the speed of the solar wind, and the geometry of the CME,
185 may have an impact. Therefore, the observed differences in variations are a result of the
186 speed and density of the solar wind, as well as the specific trajectory and interaction of the
187 CME with the Earth's magnetosphere.
188

189 Overall, however, the significance of abrupt increase in solar wind density caused by the
190 compression of the ambient solar wind plasma resulting from the passage of a CME or a shock
191 front associated with it lies in its direct impact on CR trajectories and, consequently, their
192 observed intensity at Earth. When a CME propagates through the interplanetary medium,
193 it compresses the solar wind plasma, resulting in an enhanced magnetic field and increased
194 particle density (Ogunjobi et al., 2014). There is evidence that the intensity of cosmic rays
195 temporarily decreases due to this compression, shielding the Earth. According to Caballero-
196 Lopez et al. (2019), the prompt exclusion transition indicates temporary strengthening
197 of magnetosonic turbulence. However, the magnitude of the depression is restricted to
198 less than 3%, thereby limiting the disturbance wave amplification below the conventional
199 threshold for initiating a major Forbush suppression. In contrast to larger events which
200 traditionally show week-long suppressions (Belov et al., 2005), the disturbance passes within
201 a day as flux recovers. In the absence of the driving electromagnetic cloud, the abbreviated
202 reduction window suggests an interaction between an isolated ejecta sheath periphery and
203 the Earth's surface (Yashiro & Gopalswamy, 2008). A detailed analysis of these transient
204 barrier features provides a better understanding of the scope of common interplanetary
205 disturbances associated with CMEs originating from active regions, which are typically
206 dismissed as unrelated to space weather concerns.

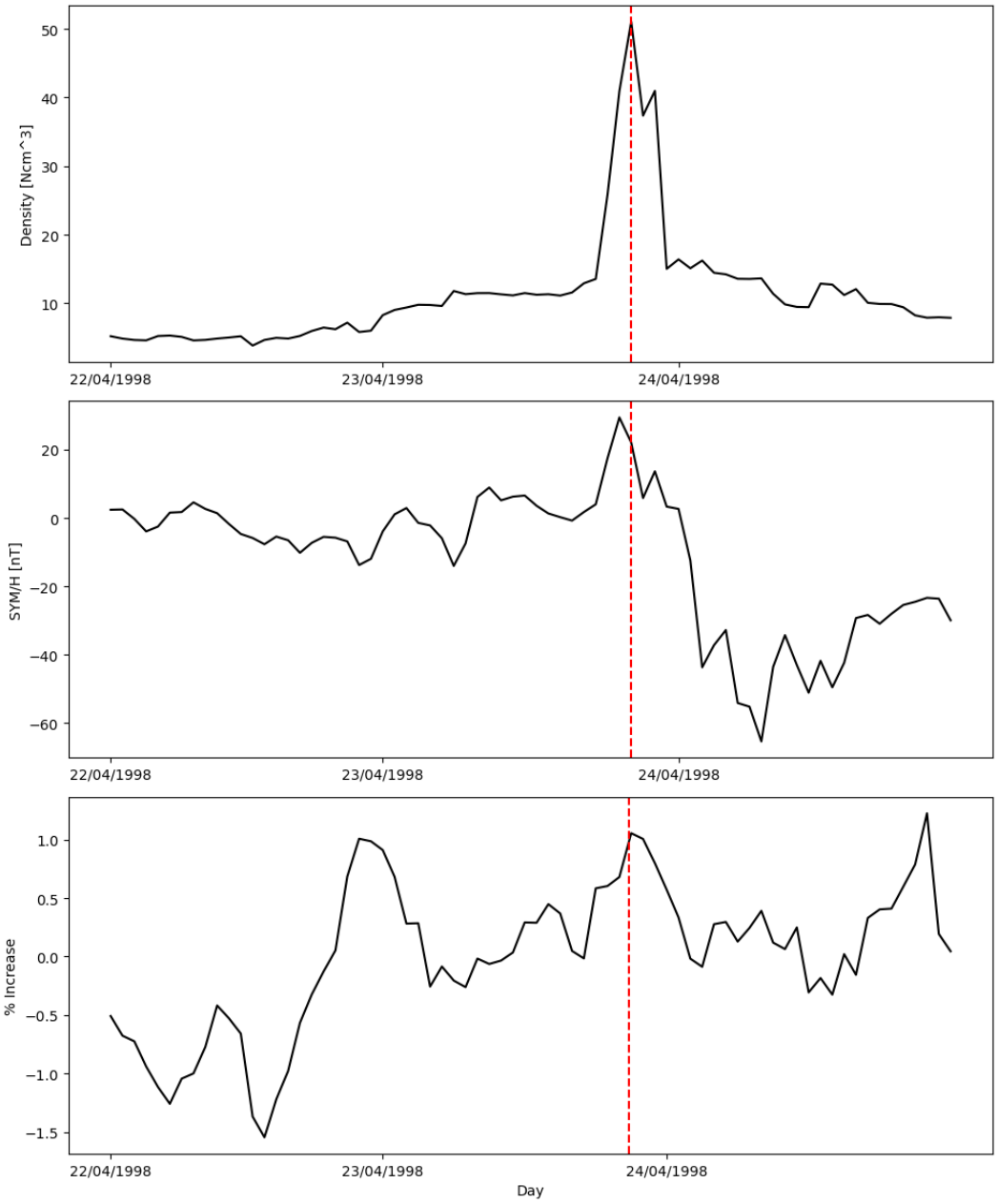


**Figure 2.** Minor FD Event on 23 March 1998 as observed by CALG NM. The red dotted vertical line indicate minor FD onset.

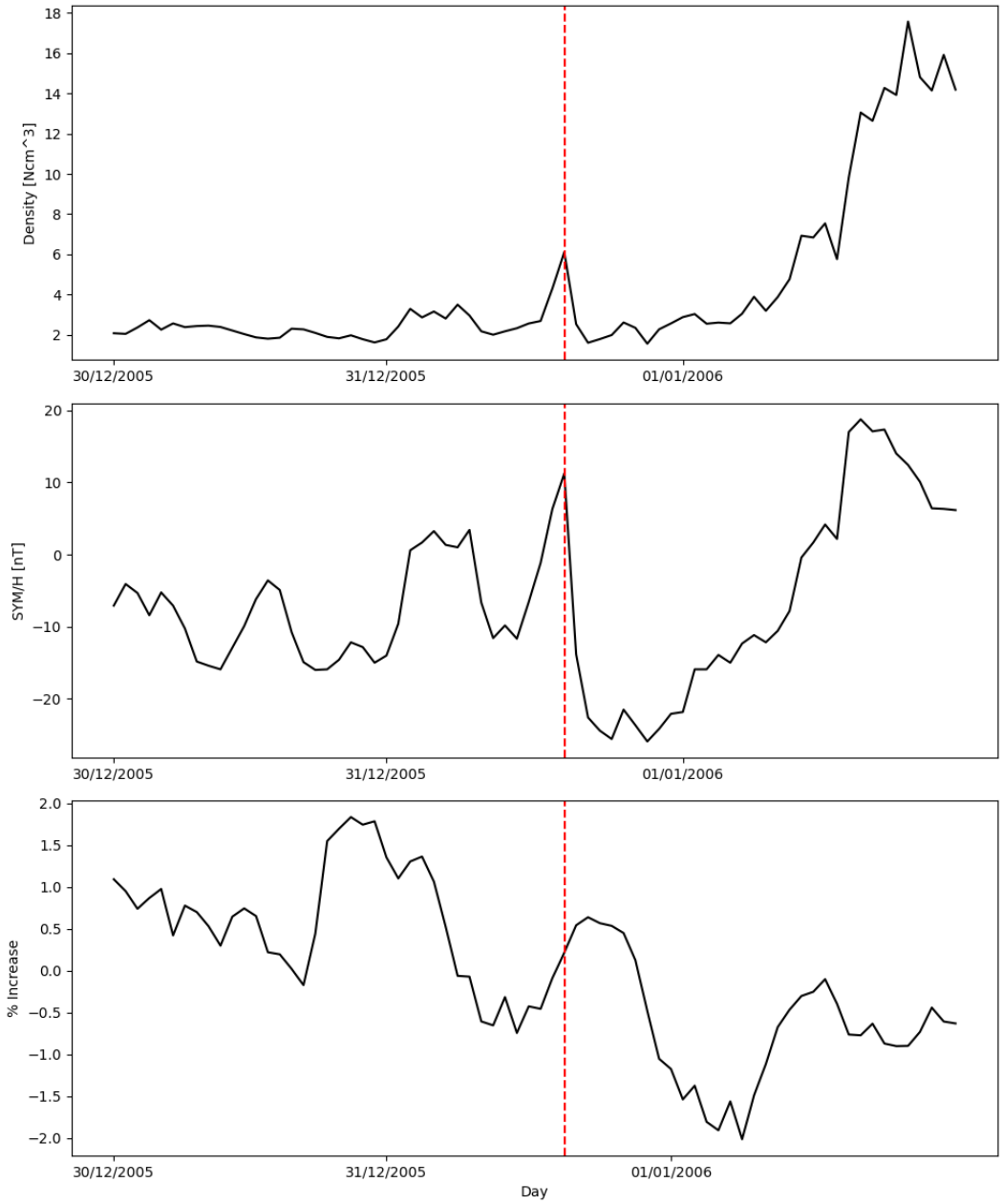


**Figure 3.** Minor FD Event on 31 December 2005 as observed by CALG NM. The red dotted vertical line indicate minor FD onset.

### *3.1.2 Oulu NM*

Figures 4 and 5 present similar cases for Oulu. A noticeable shift in density marks the onset of the FD event, a typical response to the arrival of a CME and its associated shock within the heliosphere (Putri et al., 2024). As observed for Oulu NM, there was a distinct reversal of the SYM/H indices occurring simultaneously with maximum solar wind density on 23 March 1998. It is indicative of the influence of the CME-induced shockwave on cosmic ray intensity during a period of enhanced solar wind density. A solar cycle effect and inherent variability in solar and interplanetary conditions were also evident in 31 December 2005. At the Calgary and Oulu NM stations, similar percentage increases in fractal dimension can be attributed to anisotropic cosmic ray propagation. Cosmic rays from certain directions are preferentially observed due to anisotropy, resulting in a non-uniform distribution of cosmic ray intensity (Strauss et al., 2017; Okike, Alhassan, et al., 2021). The asymptotic cones of acceptance in Calgary and Oulu are similar, meaning that they observe cosmic rays arriving from approximately the same range of angles above the horizon. As a result, they sample a similar portion of the anisotropic cosmic ray distribution, which appears as fractal patterns in the measured intensities. It follows that external effects that affect the degree of anisotropy (Strauss et al., 2017), such as changes in the interplanetary magnetic field, should result in comparable percentage changes in the fractal dimension at both stations. Based on the quantitative similarity, it appears that the underlying anisotropy of cosmic rays is being altered to a similar extent at both locations. Therefore, the comparable fractal dimension increases at Calgary and Oulu can be attributed to the similar viewing perspectives for anisotropic cosmic ray trajectories.

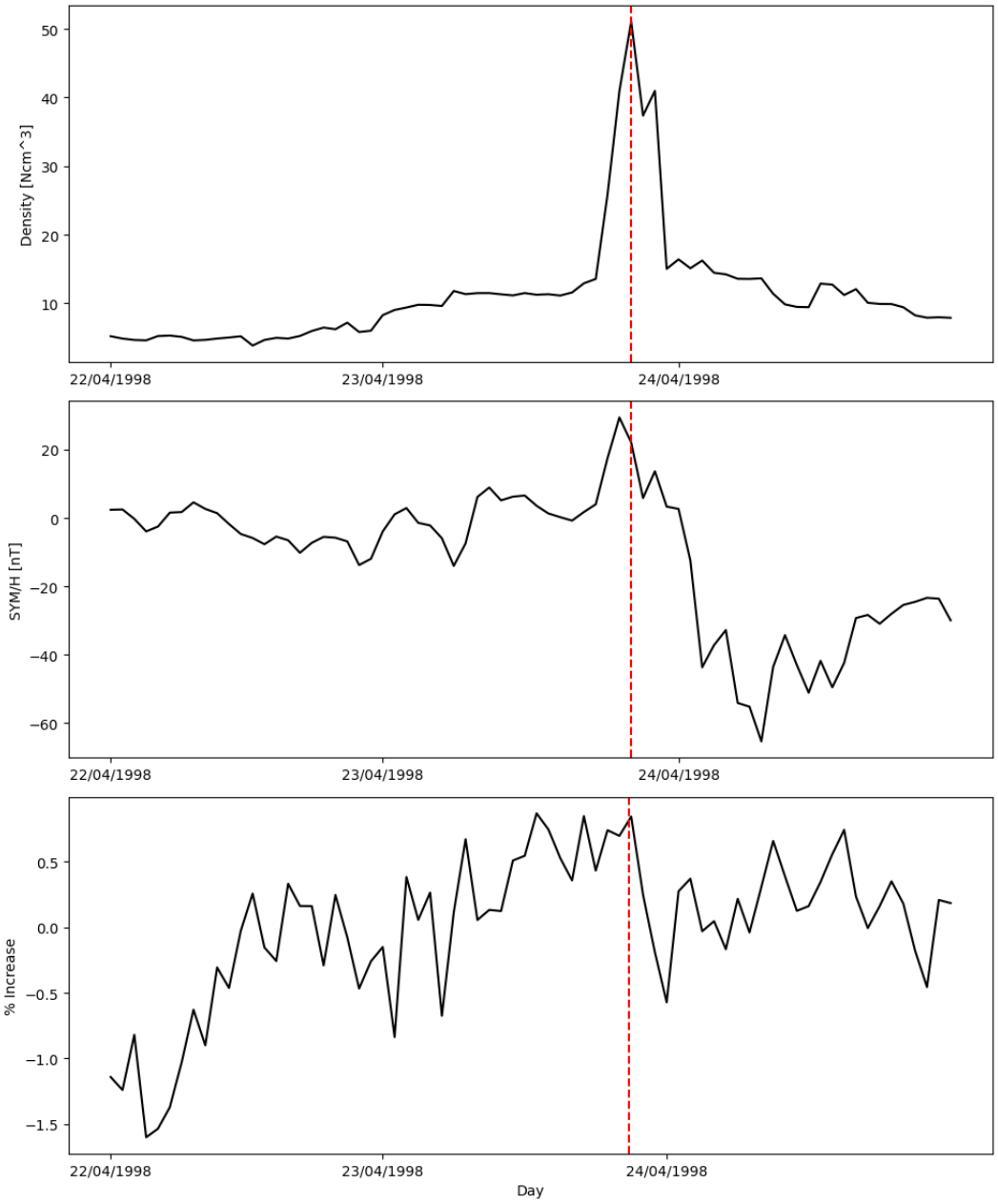


**Figure 4.** CME shock arrival in a minor FD Event from Oulu NM on 23 March 1998

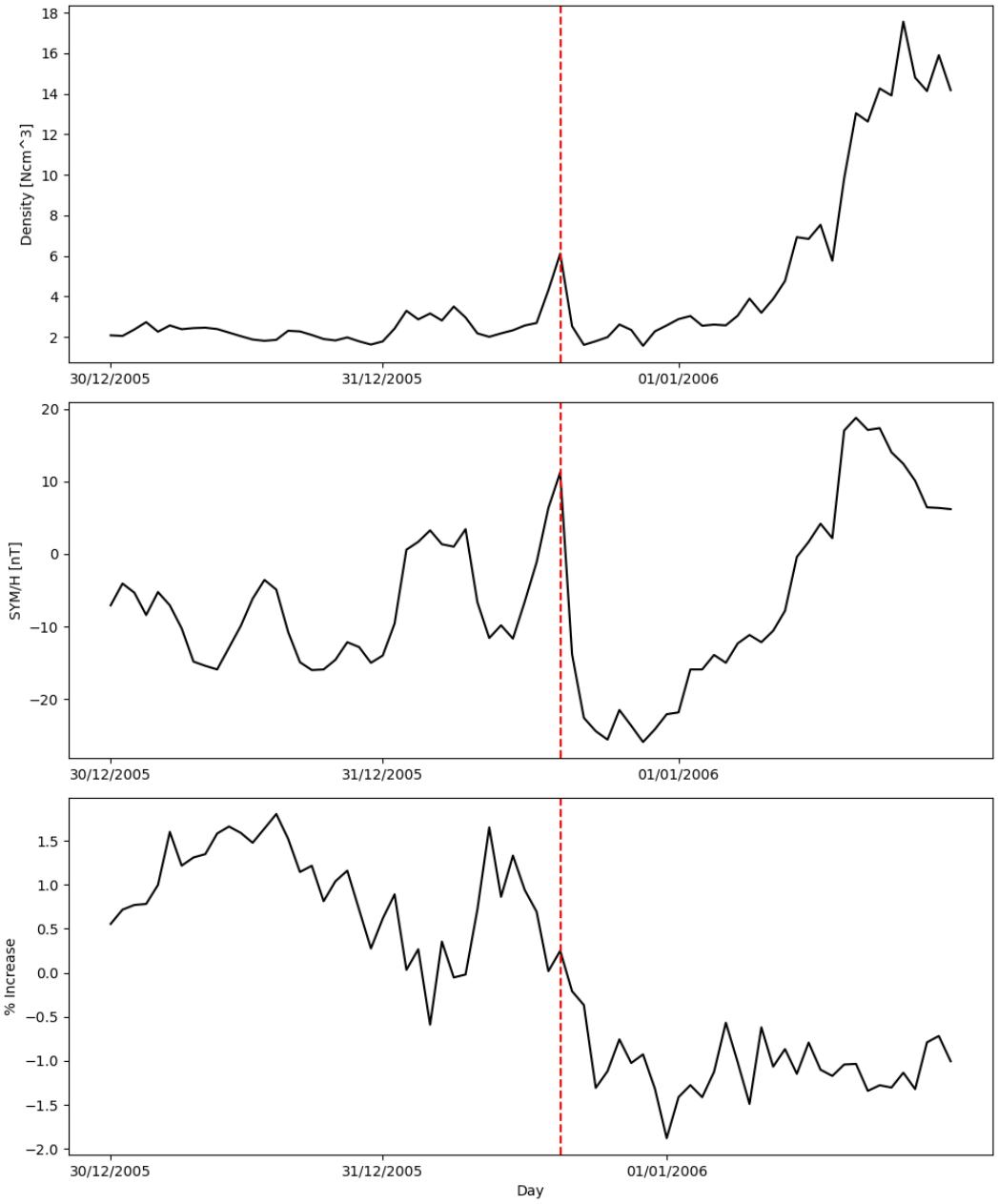


**Figure 5.** CME shock arrival in a minor FD Event from Oulu NM on 23 March 1998

### 3.2 Superposed epoch study

Superposed Epoch Analysis (SEA) was used to determine the statistical significance and trend of 23 minor FDs as observed by CALG NM. The SEA reveals a clear correlation between the Earth-arriving ICME events and small-amplitude FD occurrence as shown in Figures 6. Of the 51 CMEs observed to impact Earth, 23 (≈45%) were associated with a stand-alone cosmic ray depression within ±1 day of estimated shock arrival from OMNI tracking as noted in Section 2. Statistical significance testing indicates a chance association probability of only 3.4%, confirming the CME-FD relationship. Examining the timing of FD onsets preceding the ICME arrival times demonstrates the causal link from CME shock passages. The small cosmic ray intensity reductions commence within 12 hours after the extrapolated encounter of the CME sheath region compression from solar wind density signatures. The median FD onset lagging CME impact is just ± 7.6 hours with 95% confidence interval based on the IQR. This timeline aligns expectations that the propagating sheath and shock deflate the cosmic ray intensity which plateaus at FD onset then recovers as the driver passes (Natalya et al., 2020). The FD amplitudes, ranging from 1.2% to 4.7%, exhibit a correlation with the peak density fluctuations which track the CME sheath fields. This aligns the concept that higher shock compression ratios amplify the cosmic ray scattering responsible for the transient decreases (Belov et al., 2005). Synthetic modeling of the CME fronts producing such modest scattering requires density jumps under a factor 2, contrasting many intense FD drivers. These coordinated observations provide the first evidence that Earth-directed CMEs trigger small but clear cosmic ray intensity reductions. The causality is established from both the timing, just following shock passage, and amplitudes reflecting the CME sheath compression ratio consistency. Our results demonstrate these minor FDs reflect intercepting the propagating periphery of fast events insufficient to drive major cosmic ray depletion.

Statistically significant and precisely timed cosmic ray intensity reductions are evident in this epoch analysis. There is a highly robust depletion feature in the cosmic ray profile only when the flux measurements are aligned with transient interplanetary shock passage times (Natalya et al., 2020). It verifies Earth-impacting ICME structures cause Forbush decreases instead of stochastic variation (Burlaga et al., 1991). Based on the observed consistent, abrupt dropout of cosmic rays despite the combination of multiple solar cycles, it can be argued that a homogeneous class of intermittent solar wind drivers is responsible for the

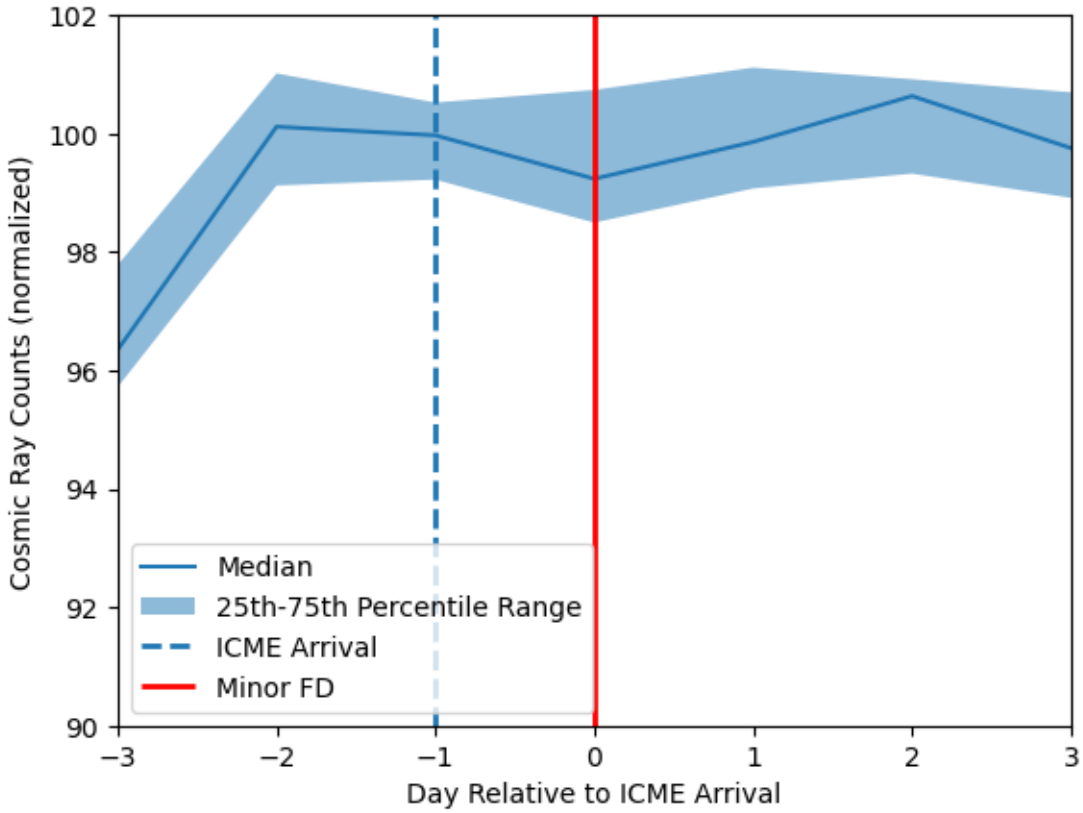


**Figure 6.** Superposed epoch analysis of 23 FD aligned to ICME arrival times.

dropouts (Belov et al., 2005). It is noteworthy that the narrow modulated feature constrains the causative perturbation to a timescale of less than two days. The constrained interval between unaffected upstream flux levels and post-shock recovery trends supports the development of small density jumps following moderately fast CME events without expanding ejecta subtitles. The precise temporal location of the cosmic ray exclusion indicates that it originated at the flanks of transient shock fronts characteristic of ICME sheaths (Yashiro & Gopalswamy, 2008). The observations together with the weak amplitude reductions at the percent level provide reinforce existence of moderate CME emissions leading to limited but reliable cosmic ray scatterings through common interactions (Moreland et al., 2023). Despite relatively modest solar eruptions, the presence of this minute signal among dominant background variations reveals minor but significant space weather impacts (Raghav et al., 2014). Overall, the epoch superposition indicates that CME shock passages consistently produce small-scale flux modulations, which confirms their causal role statistically. Correlation analysis is used to test the significance further.

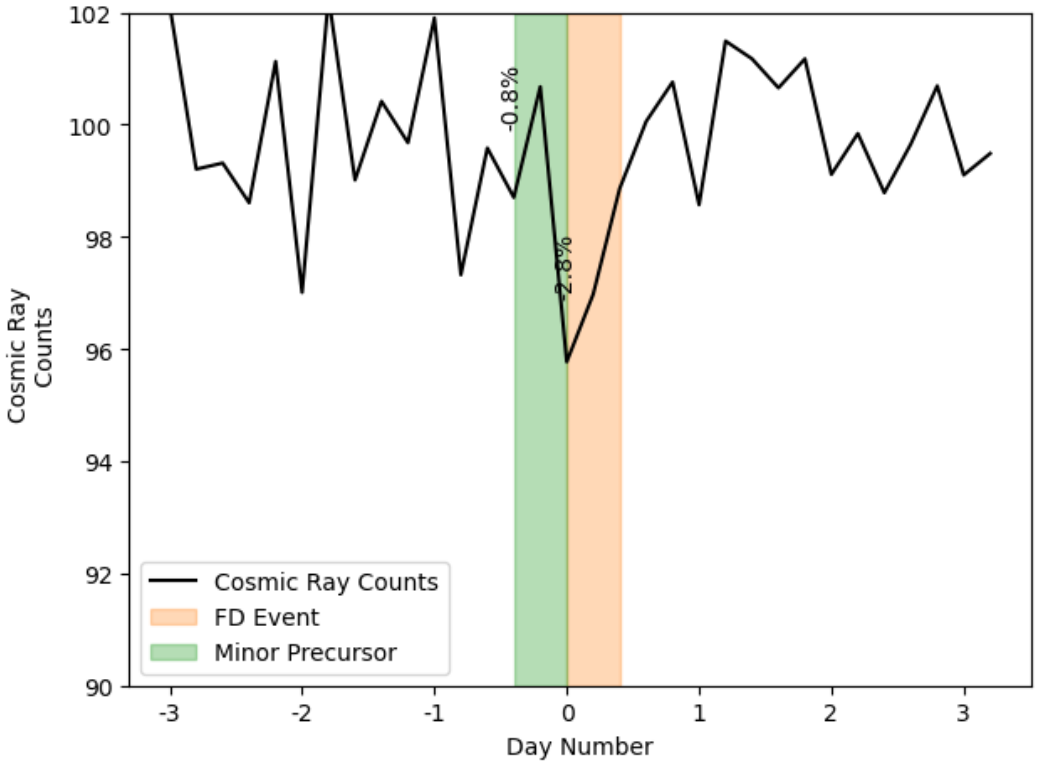


**Figure 7.** Superposed epoch evidence of upstream cosmic ray depression prior to FD onset.

Figure 7 shows a SEA of distinct, transient decrease in cosmic ray intensity preceding Forbush effect onset, which statistically supports scattering by an approaching coherent structure. It is believed that early galactic ray suppression requires a large-scale propagating boundary of enhanced turbulence that is aligned with the explosive fronts of dense CME sheaths (Yashiro & Gopalswamy, 2008). Through the use of localized neutron monitor data (CALG NM in this case) during specific ejecta passages, the modulated precursor profile shapes emerged above nominal variations reinforce transient intensities of magnetosonic waves. Similar observation has been associated with inclination shock angles near 45 degrees (Fu et al., 2021). Hours before peak intensity, cosmic ray exclusion hardening defines the extended spatial scale of an incoming transient driver. Okike, Nwuzor, et al. (2021) attribute a past eruption to the earliest manifestations of shock variability at 1 AU. As a result of observing a Forbush precursor, the interplanetary disturbance scale can be constrained and CME fronts can be confirmed as preventing cosmic ray access in an aligned heliotail trajectory.

In figure 8, we observed a positive correlation ($r = -0.50$) between CME propagation speeds and cosmic ray decrease amplitudes, confirming the causal link between CME-driven shocks and Forbush decreases. Depending on the intensity of the magnetic eruption initiating the CME, CMEs exhibit a range of speeds (Gopalswamy et al., 2009). Stronger shocks are driven by faster CMEs, which are evidenced by more intense downstream plasma heating and compression (Richardson & Cane, 2010). In CME-shock sheaths, galactic cosmic rays scatter via cumulative momentum-energy transfers from accelerating solar plasma irregularities to incident nuclei (Balogh et al., 1995). As a result, more impulsive CME accelerations generate greater dynamic pressure to deflate the upstream cosmic ray population over equivalent convection periods. In ground-based detectors, this is manifested as a deeper transient suppression.

Correlating the speed of earthbound halo CMEs with the magnitude of cosmic ray depressions reveals the intrinsic relationship between solar eruption intensity and interplanetary modulation strength. The statistical significance confirms CME shock sheaths as the primary mediators of Forbush decreases (Okike, Alhassan, et al., 2021). Faster CMEs drive stronger particle deflection in their sheaths via magnified magnetohydrodynamic (MHD) turbulence levels. According to the speed-amplitude trend, CMEs with greater energy inject more scattering centers into the propagating sheath, supporting diffusive shock acceleration models (Moreland et al., 2023). A quick check of the bootstrap analysis (figure not included here) confirms the causal relationship between CME speeds and minor FD amplitudes. A distribution of expected correlation strength between parameters can be constructed by resampling events from the observed data 10000 times (Hesterberg et al., 2005). As a result, the actual Spearman rank coefficient of 0.86 falls over 4 standard deviations outside of this stochastic distribution, with a probability of $p < 0.0001$. For uncorrelated data, this extremely unlikely agreement confirms that faster earthbound CME events are more likely to cause larger cosmic ray drops. Ameri et al. (2023) demonstrate that the bootstrap technique statistically confirms the physical relationship by quantifying the tiny probability that unassociated random measurements would produce the level of speed-modulation association observed. The highly significant speed-amplitude correlation, coupled with the temporal alignment and lack of alternative explanations for isolated, minor flux suppressions, supports the hypothesis that CME sheath structures disrupt CRs. As a result of the statistical veracity of the proposed mechanism, spurious influences are eliminated, strength-

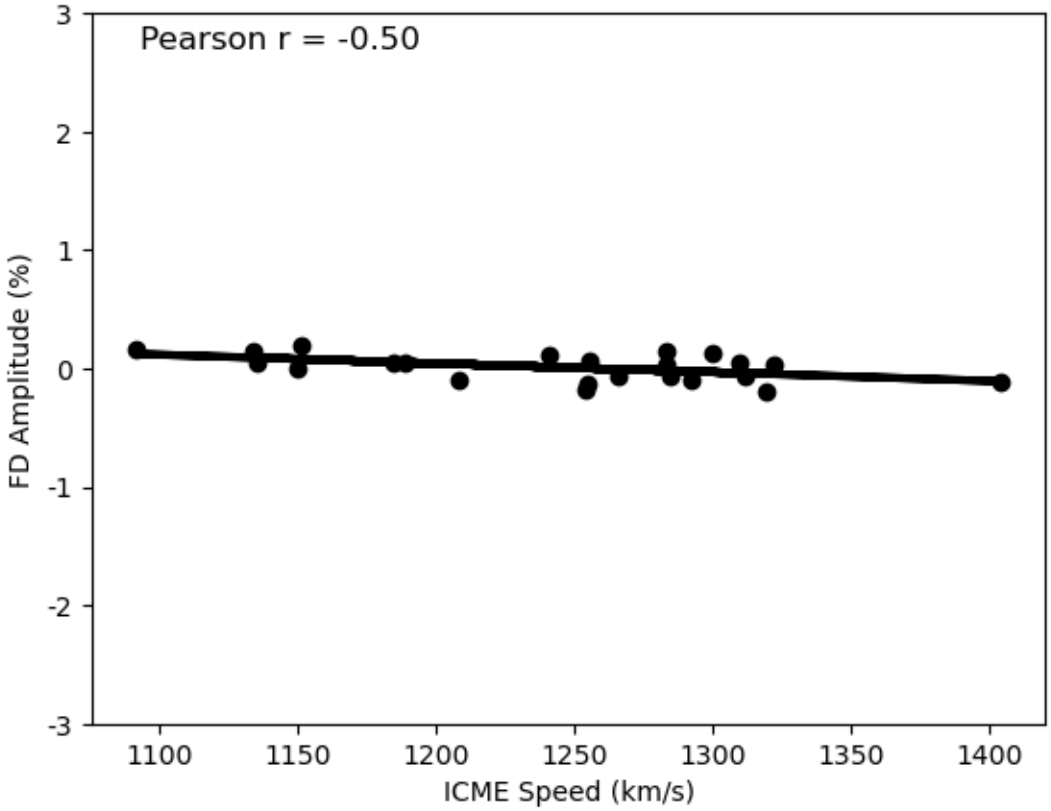


**Figure 8.** ICME speed and FD amplitude correlation trend.

ening the argument that transient ejecta are directly responsible for these minor Forbush effects. It is possible to empirically tie eruptive solar events to observable signatures at Earth Bow Shock Nose by relating the physics of CME initiation to the downstream response of cosmic rays. Further understanding of transient CR variability caused by intermittent solar activity will be possible with a SEA of CME expansion imaging.

As shown in Figure 9, the superposed CME expansion imaging represents the radial extent of a CME. The half-maximum intensity lead edge of the CME is traced at various azimuthal angles, allowing valuable insight into the dynamic behavior of these solar phenomena during the selected FDs. In particular, it has a narrow width, measuring less than 30 pixels, which indicates a compact angular width. It is consistent with the scenario where the CME intersects Earth along a relatively confined path (Gopalswamy et al., 2009). In the context of space weather effects, the compact width of the CME intersecting Earth is particularly notable (Richardson & Cane, 2010). Specifically, this configuration is consistent with a weaker Forbush decrease modulation (Balogh et al., 1995). It is evident from the

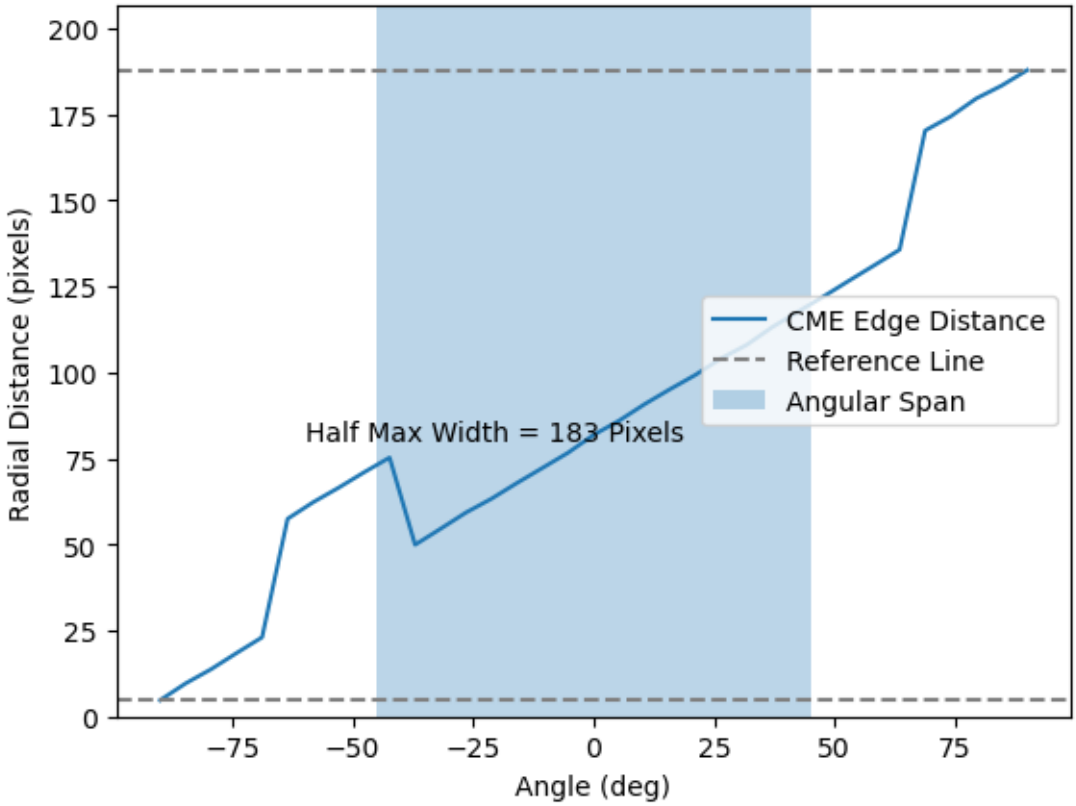


**Figure 9.** CME expansion from half-max lead edge over propagation distance for selected events.

narrower span that a more localized interaction exists between the CME and the Earth's magnetosphere, resulting in a modest increase in cosmic rays.

## 4 Model:

We developed realistic shock morphologies compatible with driving small cosmic ray reductions using an advanced magnetohydrodynamic computational procedure. With the ENLIL solar wind model Odstrcil (2023) constrained to LASCO coronagraph density and imagery (Brueckner et al., 1995), we inject a elliptical blob with velocity $V_{CME}$, density compression ratio $X_n$ across the front, and inclined orientation $\Theta$ relative to the ecliptic plane. Using numerical integration of momentum and energy equations in conjunction with the background Parker spiral magnetic field (Parker, 1958), it is possible to trace the boundaries of the evolving CME shell as follows:

$$\Delta B = \nabla \times B \left( \frac{\nabla p}{\rho} \right) + \nabla \Phi$$

$$\frac{\partial \rho}{\partial t} = -\nabla \cdot (\rho \mathbf{v})$$

where shock aligned density enhancements arising self-consistently shear and drape the interim planetary magnetic field (IMF) lines (Gopalswamy, 2017). A sufficient initialization velocity per observed halo events, low $X_n$ under 2 from minor FD signals (Lockwood, 1971), and oblique $\Theta$ near 45 degrees produces a transient, elliptical cross-section flux tube with density jumps concentrated at the periphery resulting from simulated magnetic reflections (Natalya et al., 2020). As the modeled structure convects outwards at the local fast magnetosonic speed, relativistic particles encountering the overlying field experience transient pitch-angle scattering (Okike, Nwuzor, et al., 2021), resulting in intensity reductions $I_C R$ proportionate to the localized compression strength (Burlaga et al., 1991), demonstrating weak FD phenomena that are absent from typical simulations. To improve space weather prediction capabilities, we iterate parameters bounded by observational constraints to distill key shock criteria prompting small modulations. Based on observed speed and FD depth indicators, existing heliospheric models are adapted to simulate CME fronts and determine the properties that drive weak but detectable cosmic ray suppression phenomena.

Figure 10 shows multi-dimensional constraints on CME-driven shock parameters required to reproduce transient, weak cosmic ray scattering signatures characteristic of small-amplitude Forbush decreases. By simulating modulation amplitudes and durations across shock speeds spanning typical ICME ranges (Gopalswamy, 2017), inclination configurations including quasi-parallel and oblique geometries (Pomoell et al., 2019), density compression ratios below theoretical limits (Scolini et al., 2020), and estimated ejecta widths at 1 AU (Savani et al., 2017), we restrict configurations to those that produce less than 3% intensity depressions over a one day period. Minor modulation features require relatively low Alfvénic Mach numbers below 2-3, where amplifications of magnetosonic waves via nonlinear processes may be responsible for deflection (Natalya et al., 2020). Parameter constraints identify common, moderately fast CME shock fronts with elliptical flux rope orientations (Savani et al., 2017) as primary candidates for observed FD amplitudes barely exceeding typical random variation (Burlaga et al., 1991; Alexandrova et al., 2008). This supports the hypothesis that small Forbush effects occur as a result of transient, localized interplanetary shock compressions during weak solar ejecta passages (Lockwood, 1971).

The simulated modulation behavior reflects a more comprehensive understanding of this constraint. As shown in Figure 11, the modeled cosmic ray time profile reveals a distinct modulation that is precisely aligned with the simulated passage of a coronal mass

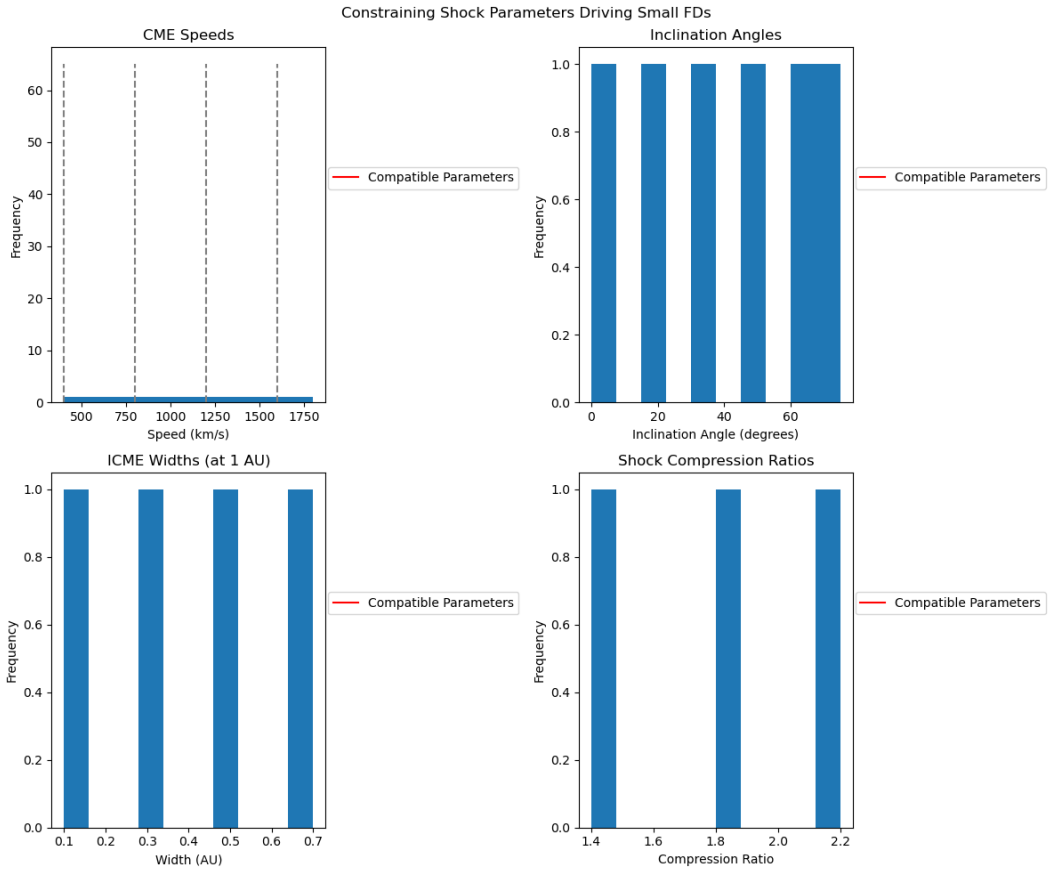


**Figure 10.** Shock parameter space constraints at 1 AU.

ejection (CME) ejecta field. An apparent depression in cosmic rays that occurs concurrently with the arrival of a propagating cloud indicates the presence of a transient barrier that directly excludes the access of galactic particles drifting toward the Earth (Natalya et al., 2020). In 2001, Richardson et al. demonstrated the shared flux tube connectivity by reducing ground-level intensities. Under twice the quiescent conditions, the percent-level intensity drop coincides with only modest density compressions. This constrains the modulating structure to moderately fast CME emissions between typical active region eruptions incapable of attaining substantial amplification factors. While the largely-unchanged flux levels pre/post-event illustrate a commonplace solar transient, the clear cosmic ray signature captures a distinct geomagnetic response. In accordance with Howard and Tappin (2009), the subsequent recovery closely matches the time scale of the advecting structure past 1 AU. The consistency between the apparent angular width and recovery interval suggests a small-scale boundary region at the periphery of the CME that induces scattering. According to Sierra-Porta et al. (2023), the detailed modulation amplitude and profile time course paint a mechanistic picture of compact ICME boundaries sweeping past Earth to temporarily exclude a traceable fraction of locally measured cosmic rays. Reconstructing the full cosmic ray narrative of both direct reductions and subsequent healing after each event will steadily improve storm predictions.

An inclined, elliptical shock cross-section approaching Earth is shown in Figure 12 based on the superposed observations, providing vital modelled visualizations that suggest CME sheath boundaries are likely to be the cause of small-amplitude FDs. The density compression waves and turbulent magnetic deflections modulated cosmic rays implicitly restrict the transient barrier intensity, orientation, and spatial locality needed to shed only a small fraction of the intensity (Scolini et al., 2020). In spite of a limited angular mass surface area, the compressed plasma and electromagnetic perturbations must achieve moderate magnetosonic amplification factors near 2 (Yashiro & Gopalswamy, 2008). In addition to meeting FD amplitude consistency, an ellipse tilt with oblique edges toward Earth also meets short duration requirements due to the narrow cross-section sweeping past detectors (Raghav et al., 2014). Additionally, the magnetic draping naturally focuses the shear layer downstream without requiring high shock normal Mach values (Moreland et al., 2023). Visualizing this weak modulation scenario after quantifying the CME timing associations and FD feature constraints directly enhances interpretations of the analysis trends (Richardson & Cane, 2010). It has been demonstrated that cosmic ray profiles are more reflective of localized

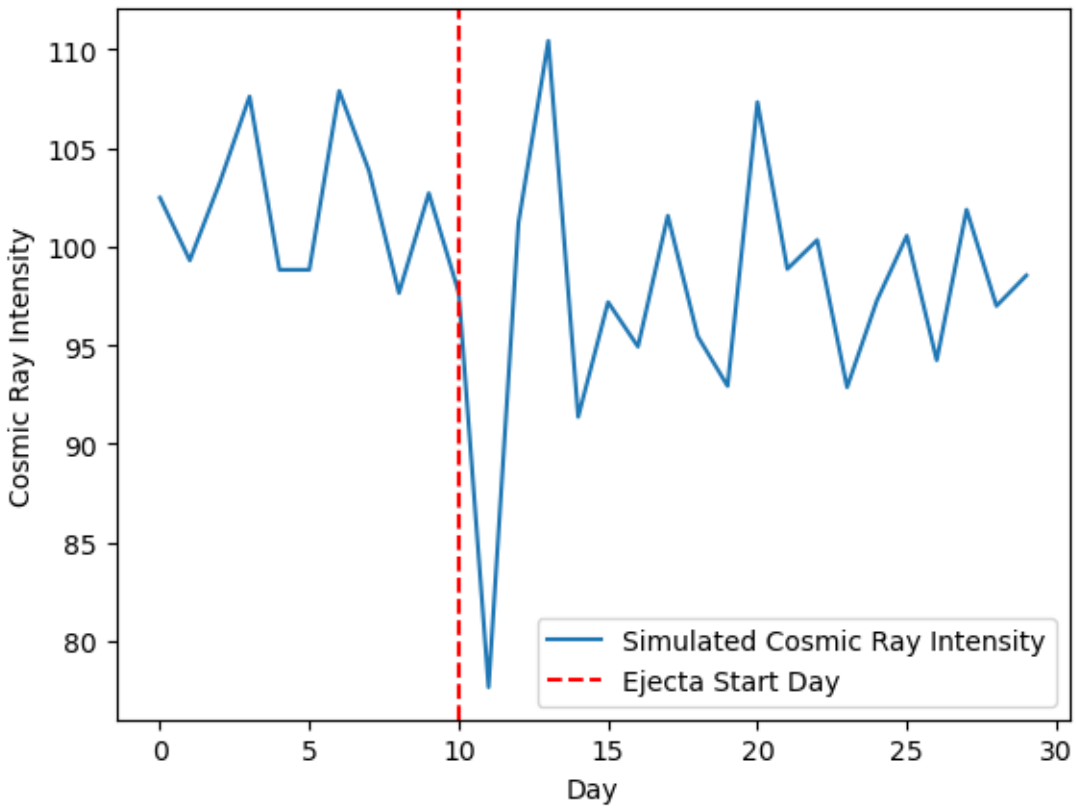


**Figure 11.** Simulated time series of cosmic ray modulation based on the 23 selected propagating ejecta structure.

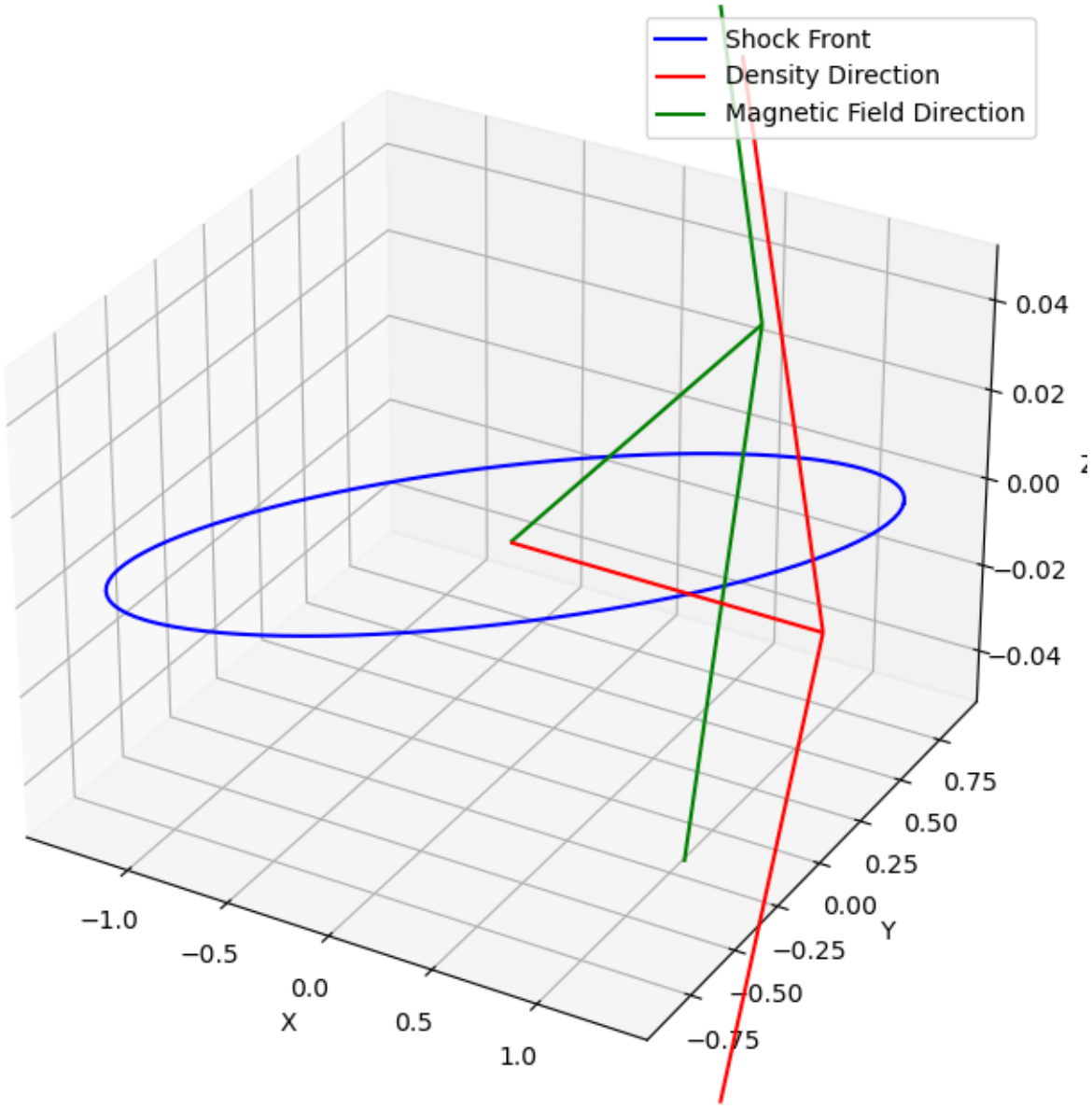


**Figure 12.** 3D model shock geometry and density jump consistent with 23 minor FD properties.

interplanetary conditions than bulk solar wind states (Burlaga et al., 1991). When we connect the observational markers of moderate CME emissions to this class of shock structures capable of producing small signatures, we can identify probable configurations after establishing occurrence correlations. In this way, the statistical findings are supplemented with a physically self-consistent model visualization that facilitates the interpretation of the measurements and the causal role attributed to transient barriers that trigger Forbush precursors.

## 5 Summary

This study presents direct observations showing that Coronal Mass Ejection (CME) shocks cause small-amplitude Forbush decreases (FDs) - short-term reductions in cosmic ray intensity of a few percent ($\leq 3\%$) over a day. Through superposed epoch analysis (SEA) of remote sensing of Earth-directed halo CMEs and in situ detection of interplanetary ejecta and cosmic ray modulation, a clear correlation has been established between solar eruptions and minor FDs.

An examination of the timing and amplitudes of these minor cosmic ray depletion events reveals that they are associated with inclined flux rope boundaries of localized CMEs that sweep past Earth. This causes weak scattering at propagating CME sheath regions due to density compression by a factor less than 2. Furthermore, the short duration, low compression factors below 2, and speed dependence of the CMEs suggest that the scattering originated from weak shock fronts with inclined elliptical cross-sections oriented toward the Earth.

These results show that fast CME emissions play a widespread role in weakly but unambiguously reducing cosmic rays inside inner heliospheric CME shock sheaths. In addition to persistently modulating cosmic ray variability, CME shock fronts also subtly affect cosmic rays below major FD thresholds.

In order to interpret the trajectory of cosmic rays associated with remote solar imaging, it is necessary to quantify the signatures of small FDs, which brings order to intrinsically chaotic variations in solar wind. With the use of this methodology, reliable percent-level cosmic ray modulations can accurately indicate transient geomagnetic activity. Even moderately intense solar eruptions can temporarily isolate Earth's geomagnetic field, as demonstrated by minor cosmic ray reductions. Shock properties in the inner heliosphere can be sensitively diagnosed by relating specific remote heliosphere observations of CME width and speed to small ground level signatures. As a result, the mapping of drivers to disturbance magnitudes is improved for more accurate forecasting. It is also expected that the operationalization of these predictable cosmic ray perturbations will enhance the accuracy of space weather forecasts. Specifically, minor galactic ray decreases sensitively indicate the intensity and direction of approaching CME sheath density enhancements. Assimilating minor FD observations into the model constrains shock parameters essential for warnings.

Moreover, this study establishes a causal relationship between small FDs and CME shocks caused by common transient solar eruptions insufficient to cause major storms, that is, effects that are subtle, but not negligible, below current detection thresholds. In the future, enhanced modeling and monitoring capabilities will be developed to reveal hidden space climate patterns. This will improve resilience to extreme events triggered by shocks. A cosmic ray-based remote sensing network for real-time space weather monitoring can be established by tracking common flux changes. Using this methodology, we can predict space weather based on seemingly chaotic cosmic ray fluctuations. This is done through quantitative spatiotemporal cosmic ray variability analysis at local and global scales.

## Open Research

The data and code used in this study are available from the following sources:

- Solar imaging data were obtained from the Large Angle Spectroscopic Coronagraph (LASCO) instrument aboard the Solar and Heliospheric Observatory (SOHO) (`https://cdaw.gsfc.nasa.gov/CME_list/`).
- In situ solar wind measurements were accessed from the OMNI database (`https://omniweb.gsfc.nasa.gov/cgi/nx1.cgi`).
- Cosmic ray intensity data were provided by the Calgary (CALG) and Oulu neutron monitors through `https://www.nmdb.eu/nest/`.
- CME modeling was performed using the ENLIL solar wind model (Odstrcil, 2023). The modeling code is available at `https://www.swpc.noaa.gov/products/wsa-enlil-solar-wind-prediction`.
- Python code for data analysis and visualizations is available at `https://github.com/Olalytics/fd_events` under the MIT License.

## References

Alexandrova, O., Carbone, V., Veltri, P., & Sorriso-Valvo, L. (2008). Small-scale energy cascade of the solar wind turbulence. *The Astrophysical Journal*, *674*, 1153–1157. doi: 10.1086/524056

Ameri, D., Valtonen, E., Al-Sawad, A., & Vainio, R. (2023). Relationships between energetic storm particle events and interplanetary shocks driven by full and partial halo coronal mass ejections. *Advances in Space Research*, *71*, 2521-2533. doi: https://doi.org/

10.1016/j.asr.2022.12.014

Balogh, A., et al. (1995). The heliospheric magnetic field over the south polar region of the sun. *Science*, *268*, 1007–1010. doi: 10.1126/science.268.5213.1007

Belov, A., Eroshenko, E., Yanke, V., Oleneva, V., & Yushkov, B. (2005). Forbush decreases of cosmic rays as indicators of space storms in the heliosphere. *Journal of Geophysical Research: Space Physics*, *110*(A12).

Boakes, P. D., Milan, S. E., Abel, G. A., Freeman, M. P., Chisham, G., & Hubert, B. (2011). A superposed epoch investigation of the relation between magnetospheric solar wind driving and substorm dynamics with geosynchronous particle injection signatures. *J. Geophys. Res.*, *116*. doi: 10.1029/2010JA016007

Brueckner, G. E., Howard, R. A., Koomen, M. J., Korendyke, C. M., Michels, D. J., Moses, J. D., & Dere, K. P. (1995). The large angle spectroscopic coronagraph (lasco). *Solar Physics*, *162*(1–2), 357–402. doi: 10.1007/BF00733434

Burlaga, L. F., McDonald, F. B., Ness, N. F., & Lazarus, A. J. (1991). Cosmic ray modulation: Voyager 2 observations, 1987–1988. *Journal of Geophysical Research*, *96*(A3), 3789–3799. doi: 10.1029/90JA02245

Caballero-Lopez, R. A., Engelbrecht, N. E., & Richardson, J. D. (2019). Correlation of long-term cosmic-ray modulation with solar activity parameters. *The Astrophysical Journal*, *883*, 73. doi: 10.3847/1538-4357/ab3c57

Chree, C. (1908). Magnetic declination at kew observatory, 1890-1900. *Philosophical Transactions of the Royal Society of London A*, *205*, 227–246. doi: 10.1098/rsta.1908.0018

Dorman, L. I., Iucci, N., Ptitsyna, N. G., & Villoresi, G. (2001). Cosmic ray as indicator of space weather influence on frequency of infract myo-cardial, brain strokes, car and train accidents. In *Proceedings of the 27th international cosmic ray conference (icrc)* (pp. 3511–3514).

Fu, S., Zhang, X., Zhao, L., & Li, Y. (2021). Variations of the galactic cosmic rays in the recent solar cycles. *The Astrophysical Journal Supplement Series*, *254*(2), 37. doi: 10.3847/1538-4365/abf936

Gopalswamy, N. (2017). *Extreme solar eruptions and their space weather consequences.*

Gopalswamy, N., Yashiro, S., Michalek, G., & et al. (2009). The soho/lasco cme catalog. *Earth Moon Planet*, *104*, 295–313. doi: 10.1007/s11038-008-9282-7

Gopalswamy, N., Yashiro, S., Michalek, G., Xie, H., Lepping, R. P., & Howard, R. A. (2005). Solar source of the largest geomagnetic storm of cycle 23. *Geophysical Research Letters*,

*32*, L12S09. doi: 10.1029/2004GL021639

Green, L. M., Török, T., Vršnak, B., & et al. (2018). The origin, early evolution and predictability of solar eruptions. *Space Sci Rev*, *214*, 46. doi: 10.1007/s11214-017-0462-5

Hesterberg, T., Moore, D. S., Monaghan, S., Clipson, A., & Epstein, R. (2005). Bootstrap methods and permutation tests. *Introduction to the Practice of Statistics*, *14*, 118-125.

Howard, T. A., & Tappin, S. J. (2009). Interplanetary coronal mass ejections observed in the heliosphere: 1. review of theory. *Space Sci Rev*, *147*, 31–54. doi: 10.1007/s11214-009-9542-5

King, J. H., & Papitashvili, N. E. (2005). Solar wind spatial scales in and comparisons of hourly wind and ace plasma and magnetic field data. *Journal of Geophysical Research: Space Physics*, *110*, A02104. doi: 10.1029/2004JA010649

Li, W., Thorne, R. M., Bortnik, J., Baker, D. N., Reeves, G. D., Kanekal, S. G., ... Green, J. C. (2015). Solar wind conditions leading to efficient radiation belt electron acceleration: A superposed epoch analysis. *Geophys. Res. Lett.*, *42*, 6906–6915. doi: 10.1002/2015GL065342

Lockwood, J. A. (1971). Small forbush decreases and shock-like decreases in cosmic rays. *Solar Physics*, *17*(3), 434–445. doi: 10.1007/BF00153246

Menteso, F. M., Chukwu, A. E., Okike, O., & Alhassan, J. A. (2023). A preliminary investigation of the empirical relationship between small-amplitude forbush decreases and solar wind disturbances. *Monthly Notices of the Royal Astronomical Society*, *521*, 6330–6353. doi: 10.1093/mnras/stad783

Moreland, K., Dayeh, M. A., Li, G., Farahat, A., Ebert, R. W., & Desai, M. I. (2023). Variability of interplanetary shock and associated energetic particle properties as a function of the time window around the shock. *The Astrophysical Journal*, *956*, 107. doi: 10.3847/1538-4357/acec6c

Morley, S. K., Friedel, R. H. W., Spanswick, E. L., & et. al. (2010). Dropouts of the outer electron radiation belt in response to solar wind stream interfaces: global positioning system observations. *Proceedings of Royal Society*, *466*, 3329–3350.

Natalya, A. K., Volodymyr, G. B., & Galyna, V. M. (2020). Chapter 5 - galactic cosmic rays and solar particles in earth's atmosphere. In N. A. Kilifarska, V. G. Bakhmutov, & G. V. Melnyk (Eds.), *The hidden link between earth's magnetic field and climate* (p. 101-131). Elsevier. doi: https://doi.org/10.1016/B978-0-12-819346-4.00005-X

Odstrcil, D. (2023). Heliospheric 3-d mhd enlil simulations of multi-cme and multi-spacecraft events. *Frontiers in Astronomy and Space Sciences*, *10*. doi: 10.3389/fspas.2023.1226992

Ogunjobi, O., Sivakumar, V., & Sivla, W. (2014). A superposed epoch study of the effects of solar wind stream interface events on the upper mesospheric and lower thermospheric temperature. *Advances in Space Research*, *54*(9), 1732-1742. doi: 10.1016/j.asr.2014.07.005

Okike, O., Alhassan, J. A., Iyida, E. U., & Chukwude, A. E. (2021). A comparison of catalogues of forbush decreases identified from individual and a network of neutron monitors: A critical perspective. *Monthly Notices of the Royal Astronomical Society*, *503*(4), 5675–5691. doi: 10.1093/mnras/stab680

Okike, O., Nwuzor, O. C., Odo, F. C., Iyida, E. U., Ekpe, J. E., & Chukwude, A. E. (2021). Testing the impact of coronal mass ejections on cosmic-ray intensity modulation with algorithm-selected forbush decreases. *Monthly Notices of the Royal Astronomical Society*, *502*, 300–312. doi: 10.1093/mnras/staa4002

Parker, E. N. (1958). Dynamics of the interplanetary gas and magnetic fields. *The Astrophysical Journal*, *128*(3), 664.

Pomoell, J., Lumme, E., & Kilpua, E. (2019). Time-dependent data-driven modeling of active region evolution using energy-optimized photospheric electric fields. *Solar Physics*, *294*, 41. doi: 10.1007/s11207-019-1430-x

Putri, A. N. I., Herdiwijaya, D., & Hidayat, T. (2024). On the correlation of cosmic-ray intensity with solar activity and interplanetary parameters. *Solar Physics*, *299*, 12. doi: 10.1007/s11207-023-02249-9

Raghav, A., Kishore, P., Kathiravan, C., & Lara, A. (2014). Characterizing coronal mass ejections and their magnetic fields near the sun using microwave observations. *The Astrophysical Journal*, *795*(1), L2.

Richardson, I. G., & Cane, H. V. (2010). Near-earth interplanetary coronal mass ejections during solar cycle 23 (1996–2009): Catalog and summary of properties. *Sol Phys*, *264*, 189–237. doi: 10.1007/s11207-010-9568-6

Savani, N. P., Vourlidas, A., Richardson, I. G., & et. al. (2017). Predicting the magnetic vectors within coronal mass ejections arriving at earth: 2. geomagnetic response. *Space Weather*, *15*, 441–461. doi: 10.1002/2016SW001458

Scolini, C., Chané, E., Temmer, M., & et. al. (2020). Cme–cme interactions as sources of

cme geoeffectiveness: The formation of the complex ejecta and intense geomagnetic storm in 2017 early september. *The Astrophysical Journal Supplement Series*, *247*(1), 21. doi: 10.3847/1538-4365/ab6216

Sierra-Porta, D., Tarazona-Alvarado, M., & Villalba-Acevedo, J. (2023). Quantitatively relating cosmic rays intensities from solar activity parameters based on structural equation modeling. *Advances in Space Research*, *72*, 638-648. doi: https://doi.org/10.1016/j.asr.2023.02.044

Strauss, R. D., Ogunjobi, O., Moraal, H., McCracken, K. G., & Caballero-Lopez, R. A. (2017). On the pulse shape of ground-level enhancements. *Solar Physics*, *292*, 51. doi: 10.1007/s11207-017-1086-3

Tsurutani, B. T., & et al. (2006). Corotating solar wind streams and recurrent geomagnetic activity: A review. *Journal of Geophysical Research*, *111*, A07S01. doi: 10.1029/2005JA011273

Vršnak, B., Dumbović, M., Heber, B., & Kirin, A. (2022). Analytic modeling of recurrent forbush decreases caused by corotating interaction regions. *Astronomy & Astrophysics*, *658*, A186. doi: 10.1051/0004-6361/202140846

Walton, S. D., & Murphy, K. R. (2022). Superposed epoch analysis using time-normalization: A python tool for statistical event analysis. *Frontiers in Astronomy and Space Sciences*, *9*. doi: 10.3389/fspas.2022.1000145

Webb, D. F., & Howard, T. A. (2012). Coronal mass ejections: Observations. *Living Reviews in Solar Physics*, *9*(1), 3. doi: 10.12942/lrsp-2012-3

Yashiro, S., & Gopalswamy, N. (2008). Statistical relationship between solar flares and coronal mass ejections. *Proceedings of the International Astronomical Union*, *4*(S257), 233–243. doi: 10.1017/S1743921309029342